quent expression of CD20 and a less-frequent expression of CD56 [4, 5]. Several myeloma studies have shown that CD20 expression is associated with small-cell-type neoplastic PCs and t(11;14) in PCM [6, 7]. As CD56 is an adhesion molecule, PCs with no CD56 expression may reduce cell-to-cell interactions, easily escape from the bone marrow, invade extramedullary organs, including the peripheral blood, and proliferate abnormally beyond immune surveillance [4, 5].

To date, only 5 cases of small-cell-type PCL (Table 1) have been reported, while clonal PCs of the small-cell-type are found only in 3.4% of PCM [7-10]. The median age of the 6 cases including ours was 70.2 years with no demographic preponderance. The 6 cases of small-cell-type PCL demonstrated a variable expression of CD20 and loss of CD56. t(11;14) (*IGH/CCND1* rearrangement), and overexpression of *CCND1* or *CCND2* was detected in 5 cases. Their secreting components were IgG or IgA with lambda or kappa light chains, including only one kappa light chain. The amount of M protein was not associated with the tumor burden. Two patients died within a year of starting chemotherapy.

In summary, we report a rare case of pPCL with t(11;14) presenting as the small-cell type. When diagnosing PCL of an atypical plasma cell type, it is mandatory to use FCM immunophenotyping for the bone marrow and peripheral blood specimens with morphology and IFE.

Jung-Ah Kim[1], Woo Yong Shin[1], Jieun Kim[1], Hae In Bang[1],
Seug Yun Yoon[2], Rojin Park[1]
[1]*Department of Laboratory Medicine,* [2]*Department of Internal Medicine, Soonchunhyang University Seoul Hospital, Seoul, Korea*

Correspondence to: Rojin Park
Department of Laboratory Medicine, Soonchunhyang University Seoul Hospital, 59 Daesagwan-ro, Yongsan-gu, Seoul 04401, Korea
E-mail: rpark@schmc.ac.kr

Authors' Disclosures of Potential Conflicts of Interest

No potential conflicts of interest relevant to this article were reported.

REFERENCES

1. Gonsalves WI, Rajkumar SV, Go RS, et al. Trends in survival of patients with primary plasma cell leukemia: a population-based analysis. Blood 2014;124:907-12.
2. Mina R, Joseph NS, Kaufman JL, et al. Survival outcomes of patients with primary plasma cell leukemia (pPCL) treated with novel agents. Cancer 2019;125:416-23.
3. Bartl R, Frisch B, Fateh-Moghadam A, Kettner G, Jaeger K, Sommerfeld W. Histologic classification and staging of multiple myeloma. A retrospective and prospective study of 674 cases. Am J Clin Pathol 1987;87:342-55.
4. Raja KR, Kovarova L, Hajek R. Review of phenotypic markers used in flow cytometric analysis of MGUS and MM, and applicability of flow cytometry in other plasma cell disorders. Br J Haematol 2010;149:334-51.
5. Pellat-Deceunynck C, Barillé S, Jego G, et al. The absence of CD56 (NCAM) on malignant plasma cells is a hallmark of plasma cell leukemia and of a special subset of multiple myeloma. Leukemia 1998;12:1977-82.
6. Robillard N, Avet-Loiseau H, Garand R, et al. CD20 is associated with a small mature plasma cell morphology and t(11;14) in multiple myeloma. Blood 2003;102:1070-1.
7. Heerema-McKenney A, Waldron J, Hughes S, et al. Clinical, immunophenotypic, and genetic characterization of small lymphocyte-like plasma cell myeloma: a potential mimic of mature B-cell lymphoma. Am J Clin Pathol 2010;133:265-70.
8. Gounari E, Kaiafa G, Koletsa T, et al. CD5+ B lymphoproliferative disorder with subsequent development of plasma cell leukaemia: diagnostic and aetiologic reasoning. Cytometry B Clin Cytom 2018;94:688-94.
9. Loureiro AD, Gonçalves MV, Ikoma MR, et al. Plasma cell leukemia with t(11;14)(q13;q32) simulating lymphoplasmacytic lymphoma - a diagnostic challenge solved by flow cytometry. Rev Bras Hematol Hemoter 2017;39:66-9.
10. Teriaky A, Hsia CC. Plasma cell leukemia mimicking chronic lymphocytic leukemia. Blood 2011;117:2991.

Enrichment of TP53 alterations within GCB-like DNA subclassifications of diffuse large B-cell lymphoma after transition from de-novo to relapsed or refractory disease

TO THE EDITOR: Alterations of the tumor suppressor gene *TP53* are frequent in Diffuse Large B-cell Lymphoma (DLBCL), the most commonly diagnosed blood cancer at over 30,000 diagnoses per year, and are associated with poor prognosis [1]. DLBCL has traditionally been divided into three cell of origin (COO) subcategories based on RNA expression profiles or IHC: Activated B-cell (ABC), Germinal Center B-cell (GCB), and Unclassified cases [2]. Patients with ABC tumors are characterized by a more aggressive profile alongside active NF-κB and BCR signaling pathways, while GCB cases are associated with alterations that drive aberrant chromatin-modification, PI3K signaling, and the upregulation *MYC* and *BCL2* through structural variants

[3]. Both subtypes are associated with worse outcomes if impaired *TP53* is present, although these alterations do not enrich in one subtype vs. the other [1]. Recently, new classification models have utilized previously-identified DLBCL driver DNA alterations to categorize de-novo tumors into subsets [4-7]. All 3 models, supervised or unsupervised, produce a GCB-like classification: EZB (Schmitz/Wright), BCL2 (Lacy), and C3 (Chapuy). These tumors are defined by alterations significantly enriched in aggressive cases of GCB DLBCL: *CREBBP, BCL2* (mutation or translocation), *EZH2, KMT2D*, and *TNFRSF14*.

Although EZB tumors have an overall favorable prognosis

when treated with frontline RCHOP regimens, DLBCL patients that refract therapy or later relapse face a dismal outlook, with only 20% predicted to survive after 5 years, and few studies have examined the molecular landscape of relapsed or refractory DLBCL (rrDLBCL) [8]. The 2019 analysis by Rushton and colleagues analyzed the largest single rrDLBCL cohort, identifying several emergent genetic differences between rrDLBCL and de-novo tumor populations [9]. Importantly, the landmark FDA approval of Chimeric Antigen T-cell (CAR-T) therapy makes characterizing the genomic landscape of rrDLBCL a priority. Herein, we present data supporting that increased *TP53* alterations
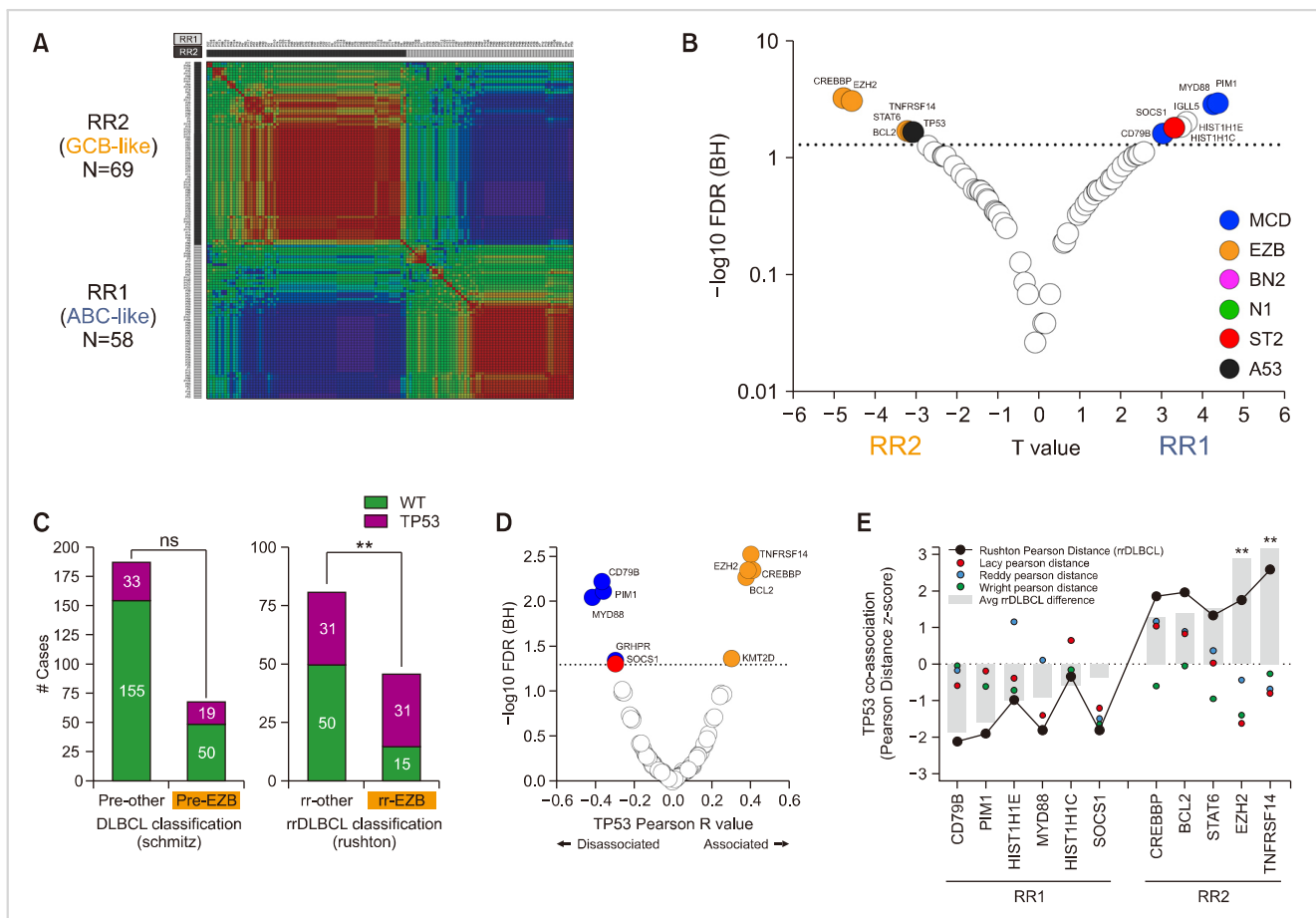

Fig. 1. *TP53* alterations enrich within GCB-like DNA subclassification alterations and rrDLBCL patients compared to de-novo cohorts. **(A)** K2 (2-cluster) NMF clustering. rrDLBCL patients (N=127) were analyzed for the best fit when measuring the association patterns of DNA alterations (N=91). Patient similarity is designated by color, with red representing the most co-association and blue the least. The RR1 and RR2 subsets that emerged from clustering are designated by light grey and dark grey coloring, respectively. **(B)** A volcano plot displays differentially enriched DNA alterations between RR1 and RR2. Comparative marker selection between the groups resulted in 2-sided T and FDR values. Greater T values were associated with RR1 and lesser values with RR2. The dotted line represents the 0.05 FDR threshold to be met for significant association with one family over the other. Significant alterations are color coded for their corresponding LymphGen cluster, if designated. **(C)** TP53 alterations are significantly enriched towards EZB tumors in rrDLBCL but not in de-novo DLBCL. Stacked bar graphs denote the presence of TP53 alterations within EZB and non-EZB tumors. The pre-treatment Schmitz *et al.* 2018 [3] cohort is compared to the Rushton *et al.* [9] rrDLBCL cohort. Significance was determined with a Fisher's Exact test within both groups. **(D)** TP53 Alterations significantly co-occur with EZB alterations and significantly occlude MCD alterations. A volcano plot displays TP53 Pearson distance for measured rrDLBCL genes. FDR-corrected correlation similarity values are plotted on the Y-axis, with FDR <0.05 noted with a dotted line. Genes are labelled and noted for LymphGen subclassification. **(E)** RR2 driver genes increased association with TP53 alterations in comparison to pre-treatment association measurements. Z-score normalized Pearson Distance values are plotted on the Y-axis against RR1 and RR2 genes on the X-axis. rrDLBCL associations (Rushton) are compared to 3 separate de-novo cohort values (Lacy, Reddy, and Wright) based on TP53 co-association. Two-way ANOVA analysis was used to measure significance between pre-treatment and rrDLBCL values after Bonferroni multiple comparison correction.

in rrDLBCL are enriched towards GCB-like subclassified cases, such as EZB, and co-associate with related DNA alterations significantly more than they do in de-novo populations.

MATERIALS AND METHODS
Data collection and NMF clustering

DNA-sequencing data from the Rushton rrDLBCL analysis (N=127) and 3 de-novo analyses were assembled (N=2,128) [4, 5, 7, 9]. These alterations designated COO via standard gene expression panels, Nanostring, the Hans algorithm, or a combination. Cases within each population were DNA-alteration classified by their respective methods or relied on the LymphGen algorithm. DNA Alterations present in less than 5 cases and patients with less than 2 alterations were filtered out. De-novo patients were filtered out of survival analyses if they were not treated with RCHOP or arose from transformation. DNA alterations included missense, deletion, frameshift, high-impact splice, and truncations. A GCB rrDLBCL validation cohort combining results from four sequencing studies was also assembled (N=54) [10-13]. The rrDLBCL population was analyzed using the Broad Institute's GenePattern Non-negative Matrix Factorization (NMF) module with assigned cluster values up to 8 [14]. Two groups emerged from this analysis – designated RR1 and RR2. FDR-corrected Marker Selection was applied to uncover differential presence of DNA alterations, with values $P<0.05$ considered significant. Pearson distance and similarity analyses to *TP53* alterations were performed using the Morpheus tool.

Statistical analyses

GraphPad Prism software and GenePattern tools were used to plot and format figures, and analyze data. Analyses were performed by Welch's t-tests, Holm-Šídák's multiple comparisons-corrected One-way ANOVA tests, and Fisher's exact tests. *TP53* alteration Pearson distances were converted to Z-scores for cross-study comparison. All reported *P*-values were two-sided and considered statistically significant below 0.05.

RESULTS
TP53 alterations enrich within the GCB-like subset of rrDLBCL patients and associate with EZB alterations

We integrated patient and targeted sequencing panel data from the Rushton analysis into 127 profiles (Supplementary Fig. 1). Unsupervised NMF clustering was applied to the cases, producing the highest cophenetic values when tumors were grouped as 2 clusters (0.9215) (Fig. 1A, Supplementary Fig. 2) (Supplementary Table 1). The 2 clusters were categorized as RR1 (N=58) and RR2 (N=69). Differential Marker Selection revealed that 13 of the 91 gene alterations were significantly enriched within either group (FDR <0.05) (Fig. 1B, Supplementary Tables 2, 3). Patients within the RR1 family were associated with *MYD88, PIM1, IGLL5, HIST1HC, SOCS1, HIST1H1E,* and *CD79B* alterations. Patients within the RR2 family were associated with

CREBBP, EZH2, STAT6, BCL2, TNFRSF14, and *TP53* alterations. Double/Triple-hit structural variations were also associated with RR2 family tumors (*P*=0.0391) (Supplementary Fig. 3). RR1 was heterogenous in its composition, harboring MCD/ABC or BN2/Unclassified tumors, while RR2 was more homogenous, composed primarily of EZB/GCB classified tumors (Supplementary Fig. 4).

TP53 alterations were significantly enriched within EZB-designated rrDLBCL cases compared to de-novo EZB cases (*P*=0.0018) (Fig. 1C). *TNFRSF14, EZH2, CREBBP, BCL2,* and *KMT2D* alterations significantly co-occurred in tumors bearing altered TP53 (Fig. 1D) after Pearson similarity matrix analysis (Supplementary Fig. 5, 6, Supplementary Table 4). In contrast, *CD79B, PIM1, MYD88, GRHPR,* and *SOCS1* alterations were significantly exclusionary of *TP53*. Z-scored Pearson distance values from *TP53* also displayed collective shifts away from RR1 genes (ABC-like) and trends towards RR2 genes (GCB-like) when compared individually (Fig. 1E) and collectively to de-novo levels (Supplementary Fig. 7, Supplementary Table 5). Specifically, rrDLBCL *TP53* associations significantly associated with *EZH2* (*P*=0.0156) and *TNFRSRF14* (*P*=0.0073).

TP53 rrDLBCL enriches towards EZB/GCB-like alterations and cases in multiple rrDLBCL cohorts and is associated with inferior RCHOP response within EZB and BCL2 subsets

We next isolated EZB-associated genes to compare *TP53*-impairment differences between de-novo analyses and rrDLBCL cases. Collective EZB Z-score association with *TP53* alterations was significantly greater in the rrDLBCL cohort compared to de-novo cohorts (*P*=0.0166) (Fig. 2A). *TP53* co-associations were next compared across all LymphGen-subsets. EZB genes harbored a significantly greater *TP53* co-association than genes associated with the MCD (*P*=0.0026), BN2, (*P*=0.0237) or unclassified (*P*=0.0017) classifications in rrDLBCL (Fig. 2B). This significant trend was observed once more within a second population of rrDLBCL patients (N=44) (Fig. 2C) [10]. We added cases to this rrDLBCL validation population, integrating Greenawalt, Morin (N=25), Juskevicius (N=21), and Jain (N=24) (Supplementary Table 6) [10-13]. Significant enrichment of *TP53* alterations within GCB cases were noted for both rrDLBCL populations (Fig. 2D, Supplementary Fig. 8). As a final measure of *TP53*-impairment's role driving refractory cases of GCB-like subclassified tumors, Kaplan-Meier survival analyses revealed significantly inferior patient survival within both when *TP53* alterations are present before RCHOP treatment (Fig. 2E). These data inform that the detrimental role of *TP53* impairment at diagnosis rises within GCB-related subclassifications of rrDLBCL.

DISCUSSION

Impairment of the *TP53* tumor suppressor is one of most negative prognostic indicators of DLBCL, strongly associat-
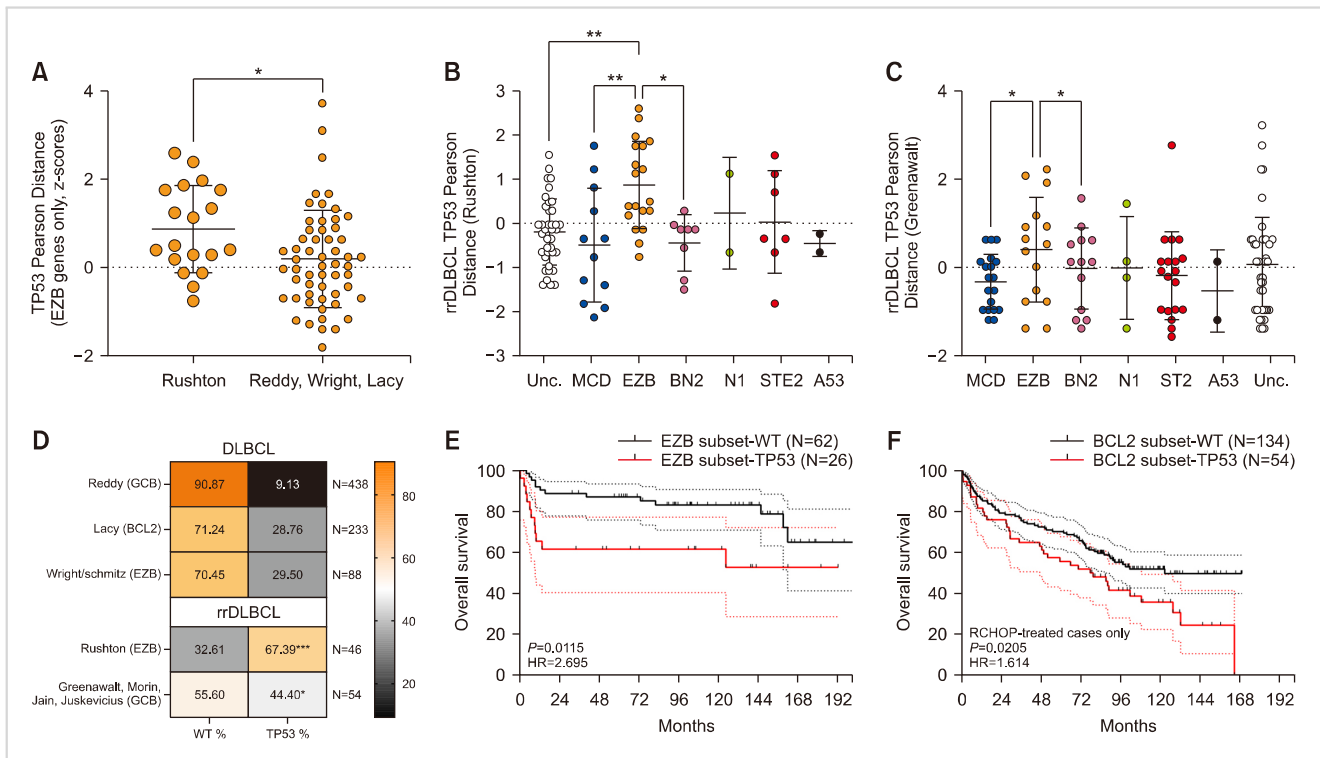
Fig. 2. *TP53* rrDLBCL enriches towards GCB-like subclassification alterations and cases in multiple rrDLBCL cohorts and is associated with inferior RCHOP response within de-novo EZB and BCL2 Subset patients. **(A)** A dot plot summarizes the Z-score normalized TP53 alteration Pearson Distance values of EZB classifier genes in the rrDLBCL population vs. combined de-novo DLBCL cohort values. A Welch's t-test was used to measure significance. Mean±SD is designated by error bars. **(B)** TP53 alterations are significantly associated with EZB alterations in rrDLBCL. TP53 Pearson distance values are displayed for 90 rrDLBCL cohort genes (Z-score normalized). One-way ANOVA analysis was used to measure significance and was corrected by a Holm-Šídák's multiple comparisons test. Gene color is matched to LymphGen subclassification. Mean±SD is designated by error bars. **(C)** Gene Pearson Distance from TP53 Alterations within the Greenawalt rrDLBCL cohort (N=44). A dot plot summarizes the Z-score normalized TP53 alteration Pearson Distance values of LymphGen classifier genes of each subset. One-way ANOVA analysis was used to measure significance and was corrected by a Holm-Šídák's multiple comparisons test. Gene color is matched to LymphGen subclassification. Mean±SD is designated by error bars. Alterations present in the cohort but not included in LymphGen classification are displayed in white. **(D)** Percentage of EZB (or corresponding) cases with non-altered (WT) vs. altered TP53 in DLBCL vs. rrDLBCL populations. A gradient denotes percent composition of each population. Significance was determined through a Fisher's Exact test between TP53 alteration enrichment within EZB or GCB cases vs. Non-GCB cases. The number of GCB/corresponding cases examined is listed on the right. **(E)** The presence of TP53 alterations at diagnosis in the GCB-like subset EZB (Wright *et al.* [5]) and BCL2 (Lacy *et al.* [7]) patients is associated with inferior overall survival. Kaplan-Meier survival curves assess the overall survival impact of TP53 alteration within EZB or BCL2 populations when treated with RCHOP. Significance was measured with Logrank analysis. The 95% confidence interval for each alteration is designated by dotted lines.

ing with inferior survival and aggressive disease biology. However, DLBCL is a heterogenous disease, often the result of cumulative epistatic genetic alterations instead of a single driver. Further, recent studies have identified associated sets of genetic alterations that co-segregate into distinctive subsets, supplementing traditional disease gene expression models [4-7]. Importantly, *TP53* alterations have not found a consensus position among these subclassifications.

When focusing rrDLBCL tumors, we identified that alterations of *TP53* enrich towards GCB-like subclassifications (EZB/C3/BCL2) compared to frequencies observed in de-no-vo populations, significantly co-occurring with EZB-classified genes as well. Our analysis relied on established, unbiased methods of clustering: the Broad Institute's NMF tool, notably responsible for the Chapuy 2018 analysis that led to the C1-C5 subsets [6]. A disadvantage is that certain cases will not find a strong consensus when few alterations

are present, but we preferred an unbiased approach in favor of seed-based models. We hypothesize that *TP53* impairment may be selected for after RCHOP treatment in a portion of EZB/corresponding cases that otherwise would not be able to reject therapy, joining rrDLBCL cases that originally presented with impaired *TP53* at diagnosis. Similarly, *EZH2* was among the *EZB* genes strongly associated with TP53 impairment in our analysis, and the Reddy analysis designated GCB+*EZH2* cases as one of their low-risk classifications, indicating that a robust loss of tumor suppression may be necessary to observe progression [4]. Similarly, strong co-associations and enrichment between *TP53* and *CREBBP* alterations may hint at cooperation between the resulting pathways during transition.

Future studies should address specific caveats encountered in our report. To begin, validation among additional rrDLBCL patient cohorts remains an important follow up

for supporting these results. Equally, the lack of CNA data may preclude these cases forming their own A53/C2 cluster, but the steep overall rise in rrDLBCL *TP53* alterations should be noted as a critical factor to consider. Our secondary rrDLBCL cohort indicated that increased *TP53* alterations remain favored to enrich in GCB-designated cases, but larger populations and sequencing studies are warranted to identify de-novo EZB/corresponding patients most likely to develop *TP53*-induced relapse. Lastly, although *KMT2D* alterations were enriched and clonally stable after the rrDLBCL transition (and typically enrich in de-novo EZB/C3/BCL2 cases), the Rushton analysis did not highlight if this rise was restricted to the GCB-like subsets. Our analysis did not observe significant association with GCB-like alterations in rrDLBCL, although they did trend towards them (Supplementary Table 2). Heavy overall enrichment (64/127 patients) may have proven difficult for *KMT2D* alterations to find a consensus association with other genes. This could also indicate that their role in rrDLBCL biology is unique.

In conclusion, we report the enrichment of *TP53* alterations towards EZB/corresponding rrDLBCL tumors (and their designate alterations) during disease transition. The strong EZB/corresponding profile of our RR2 group and consequent enrichment of *TP53* alterations highlights the importance of DNA classification models and adds clarity to patterns of rrDLBCL evolution. The rising importance of liquid biopsy monitoring in rrDLBCL patients is made all the greater by the growing indication that *TP53* impairment may predict poor response to CAR-T therapy due to the introduction of immunosuppressive pathways, specifically discussed by Shouval and colleagues at the 2021 American Society of Hematology conference [15]. *TP53* mutation status, in combination with other prognostic factors, may therefore be used to identify high-risk patients prior to CAR-T treatment.

Shelby Lund, Valentine Ngisa, Kennedee Weber, Alison Rutz, Jinda Guidinger, Keenan Thomas Hartert
Department of Biological Sciences, College of Science Engineering and Technology, Minnesota State University Mankato, Mankato, MN, USA

Correspondence to: Keenan Thomas Hartert
College of Science Engineering and Technology, Department of Biological Sciences, Minnesota State University Mankato, 228 Wiecking Center, Mankato, MN 56001, USA
E-mail: keenan.hartert@mnsu.edu

Sources of Support

Acknowledgments

Authors' Disclosures of Potential Conflicts of Interest

No potential conflicts of interest relevant to this article were reported.

REFERENCES

1. Xu-Monette ZY, Wu L, Visco C, et al. Mutational profile and prognostic significance of TP53 in diffuse large B-cell lymphoma patients treated with R-CHOP: report from an International DLBCL Rituximab-CHOP Consortium Program Study. Blood 2012;120:3986-96.
2. Alizadeh AA, Eisen MB, Davis RE, et al. Distinct types of diffuse large B-cell lymphoma identified by gene expression profiling. Nature 2000;403:503-11.
3. Schmitz R, Wright GW, Huang DW, et al. Genetics and pathogenesis of diffuse large B-cell lymphoma. N Engl J Med 2018; 378:1396-407.
4. Reddy A, Zhang J, Davis NS, et al. Genetic and functional drivers of diffuse large B cell lymphoma. Cell 2017;171:481-94, e15.
5. Wright GW, Huang DW, Phelan JD, et al. A probabilistic classification tool for genetic subtypes of diffuse large B cell lymphoma with therapeutic implications. Cancer Cell 2020;37:551-68, e14.
6. Chapuy B, Stewart C, Dunford AJ, et al. Molecular subtypes of diffuse large B cell lymphoma are associated with distinct pathogenic mechanisms and outcomes. Nat Med 2018;24:679-90.
7. Lacy SE, Barrans SL, Beer PA, et al. Targeted sequencing in DLBCL, molecular subtypes, and outcomes: a Haematological Malignancy Research Network report. Blood 2020;135:1759-71.
8. Crump M, Neelapu SS, Farooq U, et al. Outcomes in refractory diffuse large B-cell lymphoma: results from the international SCHOLAR-1 study. Blood 2017;130:1800-8.
9. Rushton CK, Arthur SE, Alcaide M, et al. Genetic and evolutionary patterns of treatment resistance in relapsed B-cell lymphoma. Blood Adv 2020;4:2886-98.
10. Greenawalt DM, Liang WS, Saif S, et al. Comparative analysis of primary versus relapse/refractory DLBCL identifies shifts in mutation spectrum. Oncotarget 2017;8:99237-44.

11. Jain MD, Ziccheddu B, Coughlin CA, et al. Genomic drivers of large B-cell lymphoma resistance to CD19 CAR-T therapy. Blood (ASH Annual Meeting Abstracts) 2021;138(Suppl):42.

12. Juskevicius D, Lorber T, Gsponer J, et al. Distinct genetic evolution patterns of relapsing diffuse large B-cell lymphoma revealed by genome-wide copy number aberration and targeted sequencing analysis. Leukemia 2016;30:2385-95.

13. Morin RD, Assouline S, Alcaide M, et al. Genetic landscapes of relapsed and refractory diffuse large B-cell lymphomas. Clin Cancer Res 2016;22:2290-300.

14. Reich M, Liefeld T, Gould J, Lerner J, Tamayo P, Mesirov JP. GenePattern 2.0. Nat Genet 2006;38:500-1.

15. Shouval R, Alarcon Tomas A, Fein JA, et al. Impact of TP53 genomic alterations in large B-cell lymphoma treated with CD19-chimeric antigen receptor T-cell therapy. J Clin Oncol 2022;40:369-81.

An infant with severe hemophilia A with intracranial hemorrhage mistaken for child abuse: a case report

TO THE EDITOR: When a child has an intracranial hemorrhage (ICH), child abuse should be considered a potential cause [1]. As with any other differential diagnoses being considered, investigations must be performed to identify occult injuries when abuse is suspected [2]. Victims of abuse typically have injuries in multiple areas in various stages of healing [1]. Bruises, bites, burns, fractures, abdominal trauma, and head trauma are the most common physical findings [1]. Suspicious inflicted injuries include posterior rib fractures, retinal hemorrhages, metaphyseal or complex skull fractures, long bone fractures, and cigarette burns in infants [1]. Moreover, subdural hemorrhage in infants is highly suggestive of inflicted trauma [1].

The prevalence of ICH in children with hemophilia is approximately 12% [3], with almost all cases occurring after trauma [3]. However, patients with severe hemophilia (factor level, 0–1%) have numerous hemorrhages from spontaneous bleeding into muscles and joints and ICH, which is the most feared complication [4]. In these patients, the symptoms are headache (44.8%), vomiting (44.8%), lethargy (41.3%), convulsions (10.3%), coma (10.3%), and various neurological symptoms [5]. Herein, we report a case of an 8-month-old infant who was initially suspected of experiencing child abuse due to ICH and skull fractures. However, after laboratory examination and police investigations, he was finally diagnosed with severe hemophilia A without child abuse and managed with coagulation factor VIII. This study was approved by the Institutional Review Board of Keimyung University Dongsan Hospital (approval no. 2022-03-029) and performed in accordance with the Declaration of Helsinki.

An 8-month-old male infant visited the emergency room for status epilepticus with stupor and prolonged fever. Initial vital signs were as follows: blood pressure, 70/40 mmHg; heart rate, 182 beats/min; oxygen saturation, 56%; and body temperature, 39.1°C. Initial laboratory tests revealed the following: pH, 7.147, (reference, 7.32–7.41); pCO$_2$, 73 mmHg (reference, 42–52 mmHg); white blood cell count, 27.63× 10^9/L (reference, 6–15×10^9/L); hemoglobin, 6.4 g/dL (reference, 10.5–14.0 g/dL); mean corpuscular volume, 79.8 fL (normal value at 8 mo, 70 fL); mean corpuscular hemoglobin level, 24.3 pg (normal value at 8 mo, 23 pg); platelet count, 875×10^9/L (reference, 130–400×10^9/L); prothrombin time (PT), 14 s (reference, 10–14 s), and activated partial thromboplastin time (aPTT), 86.4 s (reference, 20.0–33.5 s); C-reactive protein level, 13.2 mg/dL (reference, <0.5 mg/dL); erythrocyte sedimentation rate, 86 mm/h (reference, 0–15 mm/h); aspartate transaminase level, 113 U/L (reference, 22–63 U/L); and alanine transaminase level, 56 U/L (reference, 12–46 U/L). Computed tomography of the brain without contrast was performed because of severe anemia, which revealed fractures of the left temporal and parietal
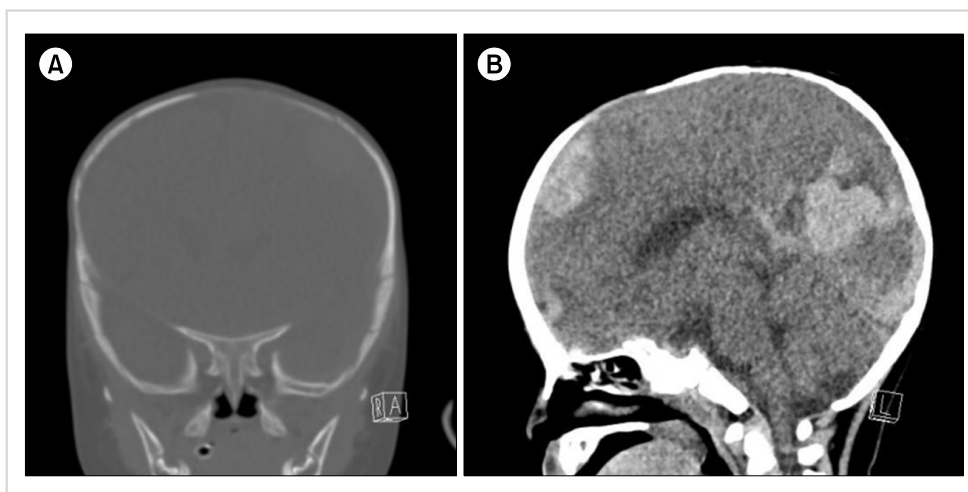

Fig. 1. Computed tomography of brain in an infant with severe hemophilia A with intracranial hemorrhage mistaken to be caused by child abuse. **(A)** Left temporal and parietal bone fractures. **(B)** Acute epidural hematoma along the entire left hemisphere and falx cerebri, multifocal hemorrhagic contusion of left cerebral hemisphere, associated subfalcine herniation, and brain edema.